Influence of Alloying Elements and Solution Heat Treatment on Microstructure and Microhardness of the Ni-Nb-*M* System (*M* = Al, Ti, Cr, Fe)

Vinicius C. Ottani[a], Mariana S. Pereira[a*] (ID), Matheus S. T. Arruda[a], Mariana C. Rossi[b], Conrado R. M. Afonso[b] (ID)

[a]*Universidade Federal de São Carlos (UFSCar), Programa de Pós-Graduação em Ciência e Engenharia de Materiais (PPG-CEM), 13.565-905, São Carlos, SP, Brasil.*
[b]*Universidade Federal de São Carlos (UFSCar), Departamento de Engenharia de Materiais (DEMa), 13.565-905, São Carlos, SP, Brasil.*

Ni-based superalloys are widely used in critical components of aircraft engines and turbines and also in the petrochemical industry, for applications in highly corrosive environments. These alloys have as main characteristics their superior mechanical, corrosion and oxidation resistance at high temperatures, as well as creep resistance. The chemical composition associated with carrying out heat treatments directly influences the phases formed (such as the ordered cubic phase γ'-Ni$_3$(Al,Ti) in the fcc γ-Ni matrix), and depending on the alloying elements and fraction, there is the possibility of an increase in mechanical strength. There is a certain gap in the literature regarding the study of ternary superalloys based on Ni-Nb, and the influence of the third alloying element on the microstructure and microhardness. In this context, the objective of the study is to characterize pseudo-eutectic alloys of the Ni-15Nb-xM and Ni-20Nb-xM systems (xM = 2Al, 4Ti, 15Fe and 15Cr, wt.%) and investigate the influence of alloy elements and solution heat treating on their microstructure and properties through X-Ray Diffraction, Optical Microscopy, Scanning Electron Microscopy and Vickers Microhardness. Microhardness and microstructures were significantly influenced by the addition of alloying elements. The addition of Cr had a significant effect on the hardness of the cast samples. All alloys showed microhardness and microstructural changes after solution heat treatment.

Keywords: *Ni-based superalloy, Niobium, Alloying elements, Microstructure, Heat treatment.*

1. Introduction

Nickel-base superalloys are an important class of high-temperature construction materials with remarkable combination of mechanical and chemical properties and have been widely used in structural components of turbine engines for propulsion and power generation[1-3]. The microstructure of Ni-base superalloys consists of an austenitic matrix phase γ and a variety of secondary phases such as gamma prime (γ') fcc ordered Ni$_3$(Al,Ti); gamma double prime (γ'') bct ordered Ni$_3$Nb, delta (δ) orthorhombic Ni$_3$Nb, eta (η) hexagonal ordered Ni$_3$Ti and other intermetallic compounds and carbides. The control of these secondary phases, grain size and morphology promote the necessary properties for the application at elevated temperatures. Topologically Close-Packed phases (TCP) σ (FeCr, FeCrMo, CrCo), μ ((Fe, Co, Nb)$_7$(Mo, W, Ni)$_6$) and Laves (Fe$_2$Nb; Fe$_2$Ti) are detrimental to the mechanical properties of superalloys. The phases σ and Laves are most often observed in iron-nickel superalloys[4].

It has been found that the major intermetallic precipitates in face-centered-cubic (FCC) IN718 matrix are mostly: (i) the body-centered tetragonal (BCT) structured (D0$_{22}$) γ''-Ni$_3$Nb phase, (ii) the ordered cubic (L1$_2$) γ'-Ni$_3$(Al,Ti) and (iii) the orthorhombic structured (D0a) δ-Ni$_3$Nb. The precipitation of γ' and γ'' phases reveal that the volume fraction and the sequence of precipitation of these two phases are controlled by the relative concentration of Al, Ti and Nb of the alloy. The precipitation of γ'' and γ' phase usually takes place at relatively low temperatures (600 - 900 °C)[5,6]. The equilibrium δ phase, however, precipitates directly from the γ matrix at temperatures above 900 °C. At temperatures below 900 °C, the metastable γ'' phase transforms to a stable δ phase over long-term exposure. The coherent γ'' is the primary phase for precipitation strengthening. Hence, the transformation of γ'' → δ may reduce the strength of IN718[5,7]. However, a moderate fraction of δ phase can improve the impact toughness[8]. Besides, the precipitation of δ phase at grain boundaries can inhibit the grain boundary sliding and thereby improves creep resistance at high temperatures[9]. It has also been proven that the presence of δ phase during hot working can avoid the undesirable grain coarsening[10].

Ni-Nb superalloys have attracted attention due to their outstanding high strength at temperatures close to their melting points due to the stability of the microstructure[11]. In nickel superalloys, niobium is normally used in concentrations between 3 and 6.3 wt.% and most of the studied alloys with emphasis on microstructure and properties consist of commercial Ni-based superalloys such as Inconel 625 and 718[12-14]. New alloys under study with higher Nb concentrations have shown superior properties. Pseudo-ternary eutectic γ-γ'-δ alloys, based on the system Ni-Nb-Al, possesses high temperature

properties compared to the commercial γ-γ' Ni-based alloys. This new class of alloys contains a large volume fraction of primary intermetallic δ-Ni_3Nb and precipitates of γ'-Ni_3(Al,Ti) as a strengthening phase. Due to the formation of the pseudo-binary γ-δ eutectic microstructure during solidification this class of alloy has high phase stability[15-18].

The development of γ-γ'-δ alloys depend on a deep understanding of microstructural evolution under extreme conditions and, consequently, of its influence on mechanical, chemical and physical properties[18]. In this way, our group studied in Afonso et al. the effects of Nb variation in the microstructure and corrosion behavior of binary Ni-xNb alloys (x = 10, 15, 20, 30, 40, 45, 52 and 57 wt %) and this work and samples were used as a reference for this research[15].

Given the above, the main objective of the study is to characterize pseudo-eutectic alloys of the Ni-15Nb-xM and Ni-20Nb-xM systems (xM = 2Al, 4Ti, 15Fe, 15Cr, wt.%) and investigate the influence of alloy elements also solution heat treating on their microstructure and properties.

2. Experimental Procedure

Initially, the Ni-Nb-*M* ternary alloys system (M = Al, Ti, Cr, Fe) were idealized to avoid the formation of TCP phases, especially Laves. The data available in the literature provided the limits for defining the chemical compositions. Thermodynamic simulations via Thermocalc also helped in the determination of TCP phase-free alloys. The compositions were based in the Ni-Nb hypoeutectic E1 field (E1 = 22.5 wt.% Nb)[15]. Samples were arc melted under argon atmosphere using non-consumable tungsten electrodes. Elements used were 99.9 wt.% electrolytic Ni, Ni-65Nb master alloy (CBMM), and high purity Cr, Fe, Ti and Al, and for the compositional balance, the calculus were based on a final ingot of 100g, thus the electrolytic Ni were added to reduce the percentage of Nb (as an example, for the Ni-20Nb-15Cr alloy, 15 g of Cr were melted with 30,77 g of Ni-65Nb - totaling 20 g of Nb - and 54,23g of Ni). The ingots were melted at least eight times to achieve high chemical homogeneity. The experimental approach that will be carried out in this project will follow the evaluated compositions shown in Table 1.

As-cast samples were submitted to heat treating to put second phases into solution, including those which are hardening phases, and so exhibit coherence with the matrix. The solution treating temperature was carried out in a Carbolite furnace, model CTF 16/50 at 1150 °C during 1 hour with subsequent water quenching. The purpose of quenching after solution treating is to preserve, at room temperature, the solid solution initially aimed, which was stable at high temperatures, and become a supersaturated solid solution after the rapid cooling.

Table 1. Nominal compositions (weight%) of Ni-*x*Nb-*M* alloys (M = Al, Ti, Cr, Fe).

Alloy	Composition (wt.%)
1	Ni-xNb-15Fe (x = 15, 20%)
2	Ni-xNb-15Cr (x = 15, 20%)
3	Ni-xNb-2Al (x = 15, 20%)
4	Ni-xNb-4Ti (x = 15, 20%)

X-ray diffraction (XRD) was performed using a Rigaku diffractometer, model Geigerflex ME210GF2, to confirm the formation of expected phases, using 2θ range from 15° to 90° at 2°/min (Bragg-Brentano reflection geometry with Cu-K_α radiation; λ = 1.5418 Å). The XRD patterns were compared with crystallographic JCPDS and ICDD data, to index all the phases present in the alloys[19,20].

Samples were cross-sectionally cut and subsequently sanded with 240, 360, 400, 600 and 1200 mesh sandpaper. After that, samples were polished using 6 μm and 1 μm diamond suspensions and 0.3 μm alumina (Al_2O_3) suspensions. Finally, chemical etching was applied with Kalling's reagent (2 g $CuCl_2$ + 40 ml HCl + 80 ml ethanol).

Metallographic characterization was carried out through optical microscopy Zeiss model Observer Z1m with AxioCamMR3 processing system. Then, characterization was completed using scanning electron microscopy (SEM) in a field emission gun - FEG microscope (Philips XL30) in SE and BSE modes, coupled to the Energy Dispersive Spectroscopy (EDS) detector, with Oxford Link Tentafet X-ray detector for chemical composition semiquantitative determination. Mechanical characterization was done through Vickers microhardness (HV), with 15 indentations in each sample in order to provide an acceptable statistical value, using a Struers Duramin-40 applying 0.5 kgf for 15 s following ASTM-E384.

3. Results and Discussion

The results of the tests described in the section above will be presented below, and then a discussion will be presented about the results found in this work and in the literature on the subject.

3.1. Microstructure characterization

3.1.1. X-ray diffraction (XRD)

Figures 1 and 2 show the XRD diffractograms of the alloys studied. In the as-cast condition the X-ray diffractograms indicate the presence of γ-(fcc), γ''-Ni_3Nb and δ-Ni_3Nb in all Ni-20Nb-xM samples; γ-(fcc) and δ-Ni_3Nb in the Ni-15Nb-15Fe, Ni-15Nb-15Cr and Ni-15Nb-4Ti and only γ-(fcc) in the Ni-15Nb-2Al. The XRD technique has a detection limit around 5% in volume[21], that is, for sufficiently low volumetric fractions and nanoscale size of precipitate, no peaks are detected in the diffractogram, even if the phase is formed in the microstructure. In this way, the conclusion is insufficient for the γ'-Ni_3(Al,Ti) and η-Ni_3Ti since these phases are usually in a low volume fraction or an a nanometric scale for Ni-Nb-Al and Ni-Nb-Ti alloys, as reported in the literature[22-24]. The precipitation of γ'-Ni_3(Al,Ti) occurs after aging and this phase will be analyzed in future works. The TCP phases σ-(FeCr) and μ-(Ni_6-Nb_7) were not identified in the X-ray diffractograms.

After solution heat treating modifications in the X-ray diffractograms were identified. There was a formation of a peak in 2θ = 34,1° but it is not possible to affirm the presence of Laves since there is an overlap with other δ-Ni_3Nb peaks. Further advanced characterization is also needed to confirm this phase. According to Tin et al.[18] due the very high stability of the primary intermetallic δ-Ni_3Nb, additional TCP phases are unlikely to form within this class of alloy. Takeyama et al.[17]
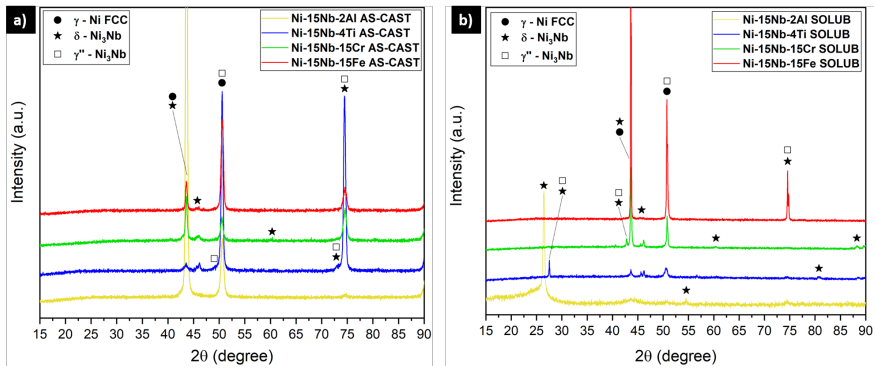
Figure 1. X-ray diffraction (XRD) diffractograms of a) As-Cast Ni15Nb-xM and b) Solution HT Ni-15Nb-xM.
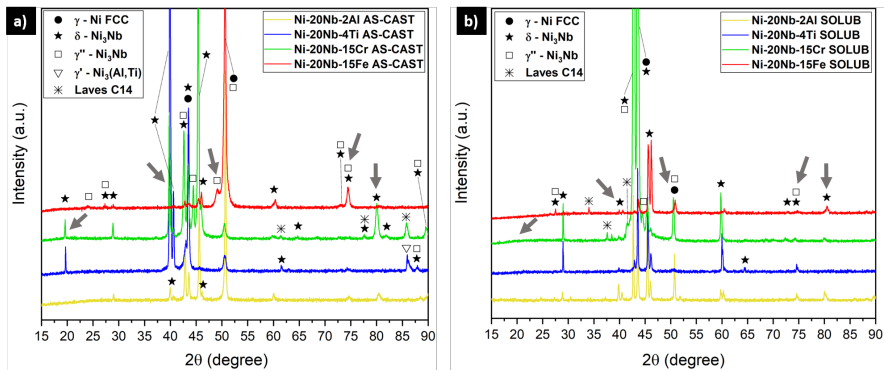
Figure 2. X-ray diffraction (XRD) diffractograms of a) As-Cast Ni-20Nb-xM and b) Solution HT Ni-20Nb-xM.

investigated the ternary Ni-xNb-Fe phase equilibria and affirmed that there is no δ-Ni₃Nb + γ-Ni fcc + C14 Laves (ε) three-phase coexisting region and it was observed a new intermetallic phase with ordered hexagonal structure (hP24 with stacking sequence of abcbcb) at compositions around Ni-22Nb-20Fe.

3.1.2. Optical (OM) and scanning electron microscopy (SEM)

A sequence of optical micrographs of Ni-20Nb-xM and Ni-15Nb-xM respectively are indicated in Figure 3 and Figure 4. As in the XRD analysis, in the optical microscope, there is a limitation regarding identifying phases with nanometric sizes since the device's resolution is approximately 400 nm. Therefore, for all the alloys in the as-cast condition it can be noted the typical dendritic microstructure of solidification. This hypoeutectic microstructure of the alloys displayed a pro-eutectic Ni-fcc phase and a (Ni + Ni₃Nb) eutectic structure. X-ray diffractograms show a higher intensity of δ-Ni₃Nb than γ''-Ni₃Nb, therefore it was expected to observe a greater volume of this phase by means of OM and SEM. Literature also confirms that such phase in this type of pseudo-eutectic alloy is δ-Ni₃Nb, since this is the stable phase formed in equilibrium solidification and γ''-Ni₃Nb is metastable. Further investigations using EBSD and TEM techniques are essential to confirm the presence of metastable γ''-Ni₃Nb, since rapid solidification in the copper ingot mold may have formed non-equilibrium phases, as observed before by Afonso et al.[15].

Samples with higher Nb concentration showed a higher volume fraction of δ-Ni₃Nb. Even though δ-Ni₃Nb was not identified by means of XRD in the as-cast Ni-15Nb-Al, a secondary phase was identified in the microstructure in very small quantities by OM. This phase is believed to be δ-Ni₃Nb due to very similar characteristics to other Ni-15Nb alloys. Fe and Cr addition also increased the volume fraction of primary δ-Ni₃Nb compared to other additions. The lowest Ni-fcc volume fraction was identified in the alloy Ni-20Nb-15Cr.

Samples Ni-15Nb-xM in the as-cast condition presented δ-Ni₃Nb with irregular morphology without presence of needle-shape precipitates (as indicated by black arrows in Figure 3). In the case of as-cast Ni-20Nb-xM samples, needle-shape δ-Ni₃Nb intermetallic (as indicated by yellow arrows in Figure 4) were identified only with Fe addition. It should also be mentioned that the δ and γ'' phases present great chemical similarity (both Ni₃Nb), and can be easily confused when using EDS and simple characterization techniques. The γ'' phase, as already mentioned, has an ordered BCT structure, it is considered a metastable phase, and coherently formed from the Nb supersaturation of the γ matrix[18]. While the δ phase is an intermetallic that can be precipitated from the matrix like the γ'', or even before the γ phase during the solidification of the Ni-Nb-M alloys, as shown through thermodynamic calculations by Xie et al.[25], presenting then distinct morphologies. This suggests that further advanced characterization is necessary to verify nature and crystalline structure associated with each of these morphologies.
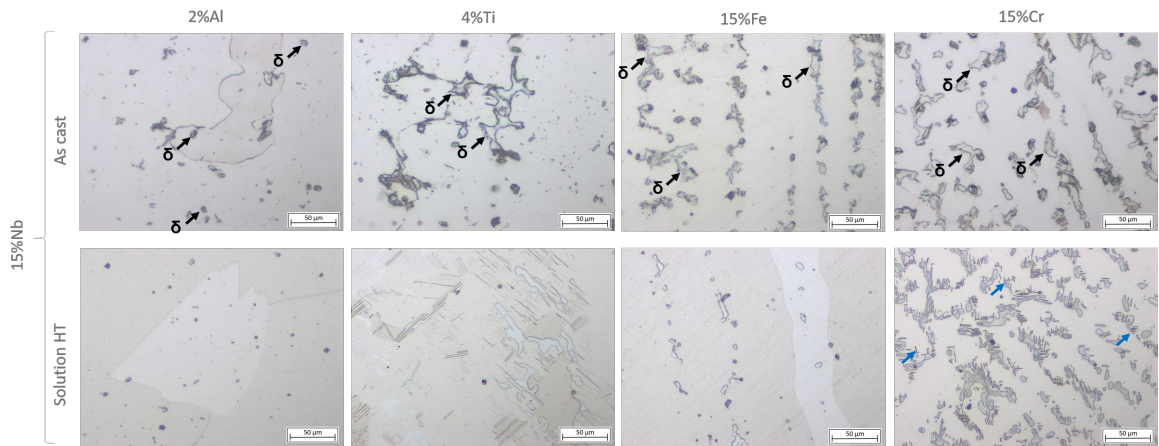
Figure 3. Optical micrographs obtained for as-cast and solution HT Ni-15Nb-xM, (xM = 2Al, 4Ti, 15Fe, 15Cr, wt.%).
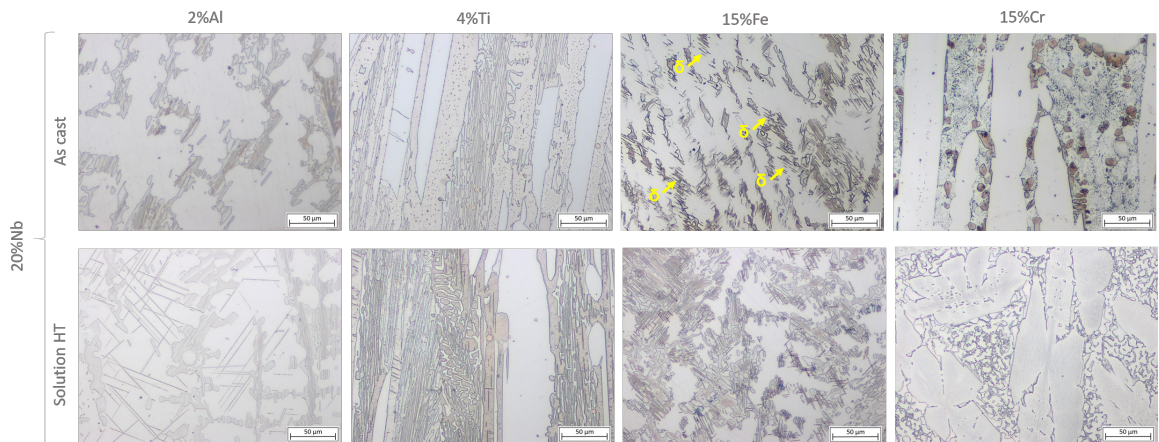
Figure 4. Optical micrographs obtained for as-cast and solution HT Ni-20Nb-xM, (xM = 2Al, 4Ti, 15Fe, 15Cr, wt.%).

The addition of Fe and Cr modified the morphologies of the phases found in the binary hypoeutectic Ni-Nb alloys. The addition of Fe to binary Ni-Nb alloys promotes the formation of metastable γ''-Ni_3Nb at relatively low temperatures[26]. Very small fractions of Ti(C,N) were identified in all samples with Ti addition, also presented in other commercial Ti alloyed Ni-base alloys. In the Ni-Nb-Ti alloys.

Microstructural changes were observed after solution heat treating. Volumetric fraction of primary δ-Ni_3Nb was reduced in the alloys in the Ni-15Nb-xM and an unexpected acicular phase was formed in the Ni-15Nb-15Cr (indicated by the blue arrow).

Chemical composition of both the alloys systems was analyzed using semi-quantitative EDS analysis. Bearing in mind that SEM/EDS is a semi-quantitative technique, and therefore a small variation is expected, the results obtained indicate that the alloys then have the designed chemical composition. The SEM micrographs of as cast Ni-15Nb-xM alloys are shown in Figure 5, where it is possible to notice different contrasts. The darker phase is the one rich in Ni, i.e. the γ matrix, and the phase shown as bright white is the one rich in Nb (the intermetallic Ni_3Nb). In addition, through the EDS analysis, it was possible to identify the presence

of segregation in the as cast samples, which is also shown in Tables 2 to 5. The presence of segregated regions on the as cast samples can be related to the rapid cooling under copper molding arc melting and lack of energy during the alloy solidification leading to the non-homogeneity of the microstructure. However, for the Ni-20Nb-xM samples, the segregation zones were not significant. The influence of alloy elements, in this case Nb could effectively decrease the solidus temperature of the alloys, affecting the solidification conditions. In the work of Xinxu[27], was reported the segregation of Ni, Al, Co, Cr and W in nickel-based superalloy.

Table 6, 7, 8 and 9 show the composition of each alloying element for the Ni-20Nb-xM system. Cr presented a limited solubility in the Ni_3Nb phase with high segregation to γ-Ni matrix. Cr additions tend to decrease solubility of Nb in the γ-Ni matrix[25]. Micrographs of as-cast Ni-20Nb-xM obtained by SEM in backscattered (BSE) mode are shown in Figure 6. It is possible to identify the needle-shape δ-Ni_3Nb in the Ni-20Nb-15Fe, high volume fraction of eutectic structure in the Ni-20Nb-15Cr, the dendritic microstructure in the Ni-20Nb-2Al with low magnification and the possible presence of Nb-Ti(C,N) in the Ni-20Nb-4Ti.
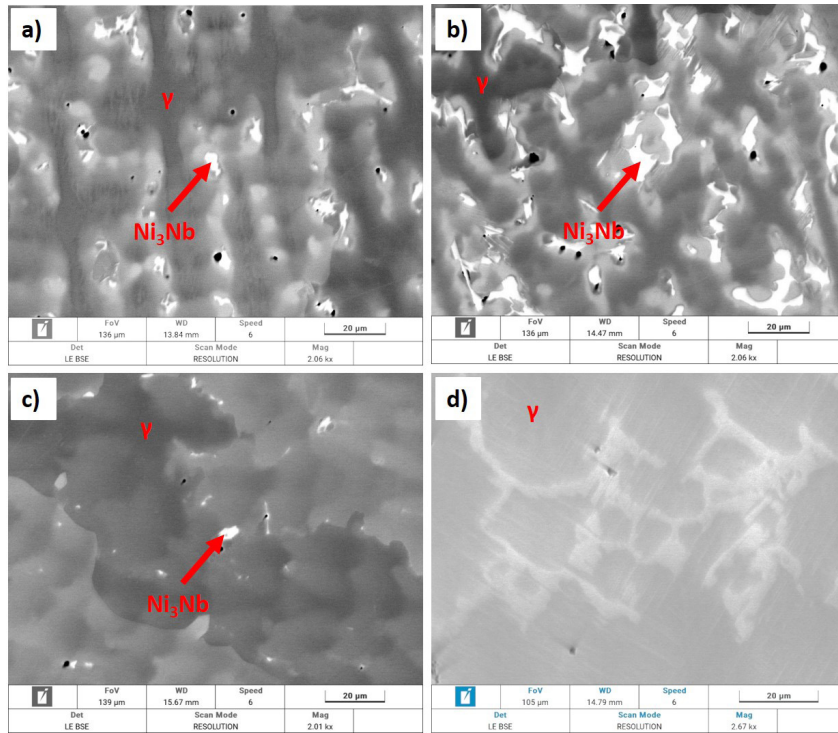
Figure 5. Micrographs obtained by SEM in backscattered (BSE) mode of (a) Ni-15Nb-15Fe, (b) Ni-15Nb-15Cr, (c) Ni-15Nb-2Al and (d) Ni-15Nb-4Ti in as-cast conditions.

Table 2. EDS semi-quantitative analysis of specific phases/regions in the microstructure of Ni-15Nb-15Fe as cast alloy.

Phase	Composition (wt.%)		
	Ni	Nb	Fe
γ (Ni fcc)	74.7 ± 1.9	5.6 ± 0.8	19.7 ± 0.6
Segregated	72.9 ± 2.2	11.8 ± 0.4	15.3 ± 0.4
Ni₃Nb	69.8 ± 0.5	21.3 ± 0.6	8.9 ± 0.3

Table 3. EDS semi-quantitative analysis of specific phases/regions in the microstructure of Ni-15Nb-15Cr as cast alloy.

Phase	Composition (wt.%)		
	Ni	Nb	Cr
γ (Ni fcc)	75.2 ± 1.9	7.3 ± 0.3	17.5 ± 0.4
Segregated	72.4 ± 1.0	10.4 ± 0.4	17.2 ± 0.3

Table 4. EDS semi-quantitative analysis of specific phases/regions in the microstructure of Ni-15Nb-2Al as cast alloy.

Phase	Composition (wt.%)		
	Ni	Nb	Al
γ (Ni fcc)	87.8 ± 2.1	10.1 ± 0.4	2.1 ± 0.1
Segregated	54.4 ± 1.8	45.2 ± 0.8	0.4 ± 0.01

Table 5. EDS semi-quantitative analysis of specific phases/regions in the microstructure of Ni-15Nb-4Ti as cast alloy.

Phase	Composition (wt.%)		
	Ni	Nb	Ti
γ (Ni fcc)	87.0 ± 2.1	9.3 ± 0.3	3.7 ± 0.4
Segregated	82.0 ± 2.0	13.0 ± 0.3	5.0 ± 0.1

Table 6. EDS semi-quantitative analysis of specific phases/regions in the microstructure of Ni-20Nb-15Fe alloy.

Phase	Composition (wt.%)		
	Ni	Nb	Fe
Ni_3Nb	64.5 ± 0.5	27.3 ± 0.7	8.2 ± 0.1
γ (Ni fcc)	67.6 ± 0.5	15.9 ± 0.4	16.5 ± 0.4

Table 7. EDS semi-quantitative analysis of specific phases/regions in the microstructure of Ni-20Nb-15Cr alloy.

Phase	Composition (wt.%)		
	Ni	Nb	Cr
Ni_3Nb	63.5 ± 0.5	31.7 ± 0.4	4.8 ± 0.4
γ (Ni fcc)	55.1 ± 1.7	11.0 ± 0.1	33.9 ± 0.7
eutectic	49.2 ± 0.4	21.4 ± 0.7	29.4 ± 0.8

Table 8. EDS semi-quantitative analysis of specific phases/regions in the microstructure of Ni-20Nb-2Al alloy.

Phase	Composition (wt.%)		
	Ni	Nb	Al
Ni_3Nb	67.8 ± 0.5	31.4 ± 0.8	0.8 ± 0.01
γ (Ni fcc)	79.9 ± 1.0	17.7 ± 0.4	2.5 ± 0.1

Table 9. EDS semi-quantitative analysis of specific phases/regions in the microstructure of Ni-20Nb-4Ti alloy.

Phase	Composition (wt.%)		
	Ni	Nb	Ti
Ni_3Nb	69.7 ± 0.5	26.3 ± 0.7	4.0 ± 0.1
γ (Ni fcc)	81.6 ± 1.9	14.5 ± 0.1	3.8 ± 0.1
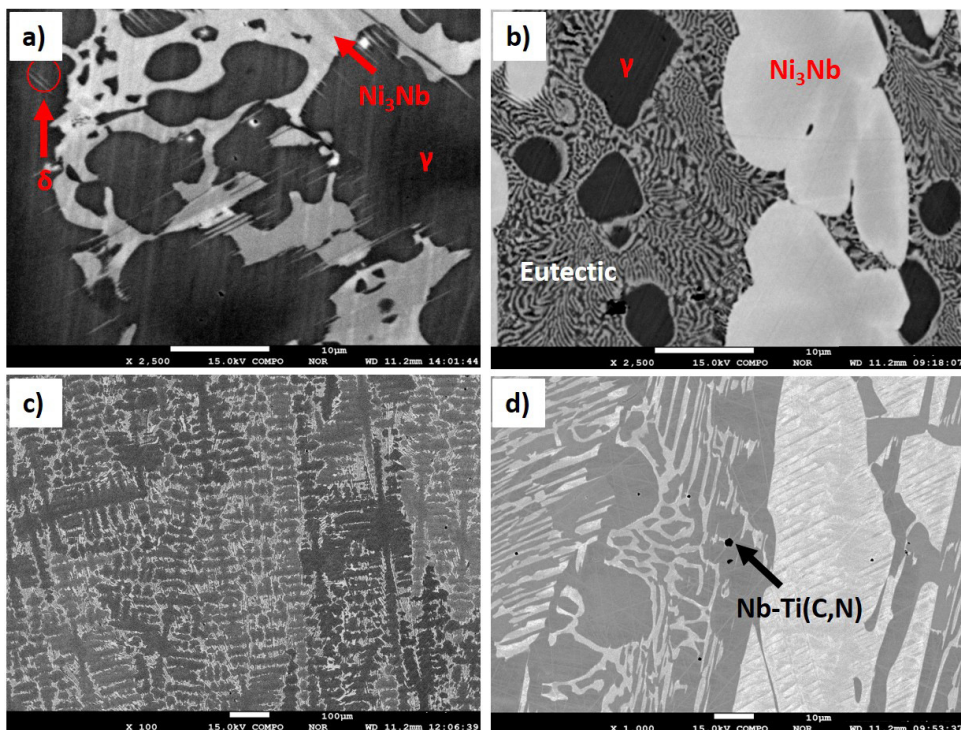
Figure 6. Micrographs obtained by SEM in backscattered (BSE) mode of (a) Ni-20Nb-15Fe, (b) Ni-20Nb-15Cr, (c) Ni-20Nb-2Al and (d) Ni-20Nb-4Ti in as-cast conditions.

Due to the similarity in principal properties, nickel and iron or nickel and chromium form a substitutional solid solution when mixed together. The Fe-Ni and Cr-Ni binary-phase diagrams, which principally represents the possible phase formation in steels alloyed with nickel, indicates the stabilization of the austenitic (fcc) phase in Ni-alloyed steel towards lower temperatures[28]. Hence, it is possible to explain the presence of Cr and Fe inside the phases reported in Table 7 (Ni_3Nb and γ-Ni).

3.2. Vickers microhardness

Figure 7 shows Vickers microhardness values of hypoeutectic binary Ni-Nb alloys were strongly altered by the addition of alloying elements. The lowest hardness among the samples, 200HV, was found in the alloy Ni-15Nb[15] and the highest hardness, 577HV, was obtained in the Ni-20Nb-15Cr alloy. The difference in microhardness after solution heat treating was lower in the samples with 20%Nb due to the lower volume fraction of γ (Ni-FCC) and greater stability of the intermetallic δ-Ni_3Nb phase.

It can be observed that for Ni-15Nb-2Al the high value of Vickers microhardness of 456 HV cannot just be attributed to a certain fraction of δ-Ni_3Nb intermetallic phase, as shown in the XRD diffractogram in Figure 1, but probably might have a significant contribution of a fraction of nanoscale γ'-Ni_3Al precipitates. But to confirm that a further investigation through TEM is ongoing in order to characterize these possible precipitates in nanoscale and even in a very small fraction. After solution HT (at T_{ht} = 1150 °C) for the Ni-15Nb-2Al alloy, the γ-Ni_3Al precipitates might have been dissolved, but instead of dissolution of δ-Ni_3Nb intermetallic phase, there was the growth of this phase fraction, clearly detected in the XRD diffractograms (Figure 1b) for Ni-15Nb-2Al alloy. Even in this way, there was a reduction of Vickers microhardness from 456 HV (as-cast) to 296 HV (after solution HT). A similar behavior happened for Ni-15Nb-4Ti with a reduction of Vickers microhardness from 386 HV (as-cast) to 311 HV (after solution HT), but in this case there was probably the formation of γ'-Ni_3Ti precipitates instead of γ'-Ni_3Al phase. And it can be seen that 2wt%Al addition (γ'-Ni_3Al phase) showed a greater hardenability (456 HV) than 4wt%Ti addition (γ'-Ni_3Ti phase) for Ni-15Nb-xM in as-cast condition.

For the solution heat treatment condition of the alloys, both for the Ni-15Nb-xM and Ni-20Nb-xM systems indicated a decrease in the microhardness. In more detail, the solubilized Ni-15Nb-xM system alloys containing 2wt% of Al dropped 35%; containing 4wt% of Ti dropped 19%; containing 15wt% of Cr dropped 39% and for 15wt% of Fe dropped 29%. The same tendency was found for the alloys of the Ni-20Nb-xM system. However, the decrease was smoother, since for the alloy containing 2wt% of Al the microhardness dropped by 7%; for the alloy containing 15wt% of Cr, it dropped by 20%; for the alloy containing 15wt% of Fe it dropped by 25%. Unlike the others, the alloy containing 4wt% of Ti did not show a significant change in microhardness after solution treatment, remaining practically unchanged. This significant decrease in microhardness can be related to the amount of primary δ-Ni_3Nb, once it was reduced after solution treatment.

Comparing now in Figure 7a the Ni-15Nb-15Cr and Ni-15Nb-15Fe alloys, it can be realized that both formed the same phases: γ-Ni matrix, γ''-Ni_3Nb and δ-Ni_3Nb intermetallic precipitates, in as-cast (457 and 321 HV) and solution HT conditions (277 and 227 HV), respectively. It can be seen that Cr addition had showed a greater hardenability in substitutional solid solution at γ-Ni matrix and also in Ni_3Nb intermetallic phases (as confirmed in EDS analysis in Tables 6 and 7), occupying the positions of Ni due to the similarity between these two elements, previously described in topic 3.1.2. Another possible factor is the fraction of eutectic microconstituent formed due to addition of 15%Cr and 15%Fe, that could be resulted differentiated and influencing the hardness of each alloy as a whole. After solution HT at 1150 °C, there might dissolved fraction of γ''-Ni_3Nb phase, decreasing microhardness of both Ni-15Nb-15Cr and Ni-15Nb-15Fe alloys and confirming that δ-Ni_3Nb intermetallic phase is much more stable at high temperature (than γ''-Ni_3Nb phase), because XRD peaks of δ-Ni_3Nb intermetallic phase (Figure 1a and 2b) were maintained after solution HT, and those peaks are more evident in XRD diffractogram for Ni-15Nb-15Cr alloy (Figure 1b).

Regarding microhardness values for Ni-20Nb-xM alloys in Figure 7b, and comparing in to groups the Ni-20Nb-2Al and Ni-20Nb-4Ti alloys as γ'-Ni_3(Al,Ti) forming alloys, with Ni-20Nb-15Cr and Ni-20Nb-15Fe alloys without formation of γ'-Ni_3(Al, Ti) phase. It can be confirmed that 2%Al and 4%Ti additions in Ni-20Nb-xM alloys in as-cast condition (Figure 2a) showed a lower capacity of dissolution of γ'-Ni_3(Al,Ti) intermetallic phase after solution HT decreasing slightly microhardness values, from 443 to 411 HV and 333 to 331 HV for Ni-20Nb-2Al and Ni-20Nb-4Ti alloys, respectively. On the other hand, for Ni-20Nb-15Cr and Ni-20Nb-15Fe alloys, there was a more significant reduction of Vickers microhardness after solution HT decreasing it from 577 to 460 HV and 463 to 348 HV for Ni-20Nb-15Cr and Ni-20Nb-15Fe alloys, respectively.
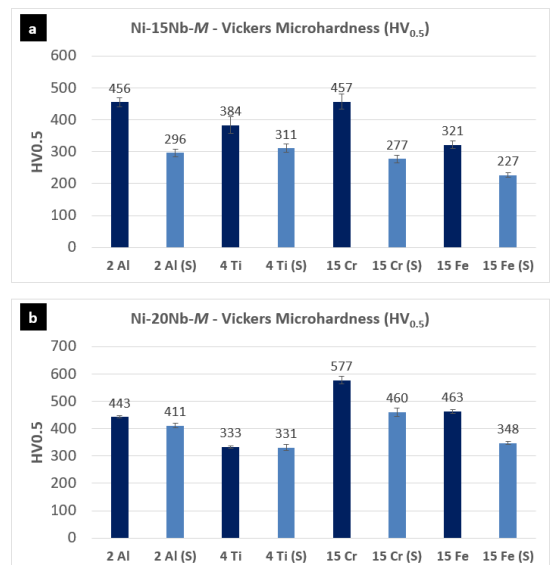
Figure 7. Vickers microhardness values $HV_{0.5}$ of (a) Ni-15Nb-xM and (b) Ni-20Nb-xM alloys in as-cast and solution treated conditions, named (S).

That can be explained by the reduction of fraction of intermetallic precipitates of γ''-Ni₃Nb and δ-Ni₃Nb phases after solution HT as indicated by the gray arrows in XRD (Figure 2a and 2b) of Ni-20Nb-15Fe and Ni-20Nb-15Cr alloys, in peaks 2θ = 19,5°, 2θ = 40° and also 2θ around 50°, 75° and 80°, where it is possible to observe a decrease in the intensity of the peaks after solution HT.

Finally, comparing the Ni-15Nb-xM system with the Ni-20Nb-xM system, it is possible to notice two general trends: i) the as cast alloys containing Al or Ti as third element, presented higher microhardness values in the Ni-15Nb-xM system, which can be explained by the lower addition of Nb, thus allowing the formation of the γ'-Ni3(Al,Ti) phase to be preferential; and ii) the alloys containing Cr or Fe showed higher hardness values in the Ni-20Nb-xM system (both for the cast alloys and for the solubilized alloys), possibly due to the greater addition of Nb, which tends to increase the precipitation of the γ''(Ni3Nb) and δ-Ni3Nb intermetallics. Also, the higher fraction of eutectic microconstituent formed and higher fraction of δ-Ni₃Nb intermetallic precipitates formed in Ni-20Nb-15Cr alloy resulted in higher hardness when compared with Ni-20Nb-15Fe alloy. That fact can be confirmed in the XRD diffractograms in Figure 2a with peaks intensity in as-cast and solution HT conditions. Another factor is the possible formation of Laves phase (Cr₂Nb type) for Ni-20Nb-15Cr alloy (as-cast and solution HT conditions) and for Ni-20Nb-15Fe alloy (Fe₂Nb type) after solution HT, which is indicated in the XRD diffractograms. But, in order to confirm the distribution of such phases in the microstructure, a deeper TEM investigation in nanoscale together with STEM-EDS elemental mapping analysis is going to be needed in order to map Laves phase in a more accurate way.

4. Conclusions

Fabrication and previous microstructural and microhardness characterization in the as cast and solubilized condition were carried out for the alloys of the Ni-15Nb-xM and Ni-20Nb-xM system, with xM being the third added element (2Al, 4Ti, 15Cr and 15Fe, wt%). From the results presented, it was possible to conclude that:

- All Ni-15Nb-xM and Ni-20Nb-xM ternary alloys systems (M = 2Al, 4Ti, 15Cr and 15Fe, wt.%) pseudo-eutectic alloys showed microhardness and microstructural changes after solution heat treatment except for Ni-20Nb-4Ti, where after solution heat treatment there was no significative difference in the microstructure value;
- The evaluated microstructure and microhardness were significantly influenced by the addition of alloying elements. Comparing the as-cast samples to heat treatment between Ni-15Nb-xM and Ni-20Nb-xM systems. Also, the addition of Cr had a significant effect on the hardness of the as-cast samples;
- The alloying elements that most contributed to increase the microhardness of the as-cast Ni-15Nb-xM alloy were Cr and Al; and in the as-cast Ni-20Nb-xM the addition of Cr provided the highest hardness among all samples;

- After solution HT, hardness of Ni-15Nb-xM was significantly decreased in all samples, mostly in the Ni-15Nb-2Al and Ni-15Nb-15Cr. In the Ni-20Nb-xM samples, solution HT had a much less significant effect on hardness, especially for the Ni-20Nb-2Al and Ni-20Nb-4Ti.

6. References

1. Donachie MJ, Donachie SJ. Superalloys a technical guide. 2nd ed. Materials Park, OH: ASM International; 2002.
2. Davis JR. ASM specialty handbook: nickel, cobalt, and their alloys. Materials Park, OH: ASM International; 2000.
3. Reed RC. The superalloys: fundamentals and applications. Cambridge: Cambridge University Press; 2006.
4. Belan J. GCP and TCP phases presented in nickel-base superalloys. Mater Today Proc. 2016;3(4):936-41.
5. Chamanfar A, Sarrat L, Jahazi M, Asadi M, Weck A, Koul AK. Microstructural characteristics of forged and heat treated Inconel-718 disks. Mater Des. 2013;52:791-800.
6. Rao GA, Kumar M, Srinivas M, Sarma DS. Effect of standard heat treatment on the microstructure and mechanical properties of hot isostatically pressed superalloy Inconel 718. Mater Sci Eng. 2003;355:114-25.
7. Liu W, Chen Z, Xiao F, Yao M, Wang S, Liu R. Effect of cold rolling on the kinetics of δ phase precipitation in Inconel 718. Metall Mater Trans, A Phys Metall Mater Sci. 1999;30:31-40.
8. Connolley T, Reed PAS, Starink MJ. Short crack initiation and growth at 600 ºC in notched specimens of Inconel 718. Mater Sci Eng. 2003;340:139-54.
9. Kuo CM, Yang YT, Bor HY, Wei CN, Tai CC. Aging effects on the microstructure and creep behavior of Inconel 718 superalloy. Mater Sci Eng A. 2009;510-511:289-94.
10. Wang Y, Shao WZ, Zhen L, Zhang BY. Hot deformation behavior of deltaprocessed superalloy 718. Mater Sci Eng A. 2011;528:3218-27.
11. Xie M, Helmink R, Tin S. The influence of Ta on the solidification microstructure and segregation behavior of γ(Ni)/γ′(Ni3Al)–δ(Ni3Nb) eutectic Ni-base superalloys. J Alloys Compd. 2012;562:11-8.
12. Tillack DJ, Eiselstein HL. The invention and definition of alloy 625. In: Loria EA, editor. Superalloys 718, 625 and various derivatives. Warrendale, PA: The Minerals, Metals & Materials Society; 1991. p. 1-14.
13. Smith GD, Patel SJ. The role of niobium in wrought precipitation-hardened nickel-base alloys. Warrendale, PA: The Minerals, Metals & Materials Society; 2005.
14. Cozar R, Rouby M, Morizot C. Mechanical properties, corrosion resistance and microstructure of both regular and titanium hardened 625 alloys. In: Loria EA, editor. Superalloys 718, 625 and various derivatives. Warrendale, PA: The Minerals, Metals & Materials Society; 1991. p. 423-36.
15. Afonso CRM, Martinez-Orozco K, Amigó V, Rovere CAD, Spinelli JE, Kiminami CS. Characterization, corrosion resistance and hardness of rapidly solidified Ni-Nb alloys. J Alloys Compd. 2020;829:1-12.

16. Takeyama M. Phase equilibria and microstructure control using δ-Ni3Nb phase in Ni-Nb-Fe ternary system at elevated temperatures. In: Chandra T, Suryanarayana C, editors. THERMEC '2000. International Conference on Processine & Manufacturing of Advanced Materials; 2001; Warrendale. Proceedings. Warrendale, PA: The Minerals, Metals & Materials Society; 2001.

17. Takeyama M, Morita S, Yamauchi A, Yamanaka M. Phase equilibria among γ, Ni3Nb-δ and Fe2Nb-ε phases in Ni-Nb-Fe and Ni-Nb-Fe-Cr systems at elevated temperatures. Warrendale, PA: The Minerals, Metals & Materials Society; 2001. p. 333-44.

18. Tin S, Rodriguez A, DiScuillo-Jones A, Helmink R, Hardy M. Polycrystalline γ-γ′-δ ternary eutectic Ni-base superalloys. Warrendale, PA: The Minerals, Metals & Materials Society; 2012.

19. CompTech. [homepage on the Internet]. [cited 2023 Jan 23]. CompTech; 2017. Available from: http://comptech.compres.us/tools/jcpds/

20. ICDD: International Center for Difraction Data. [homepage on the Internet]. ICDD; 2017. [cited 2023 Jan 23]. Available from: http://www.icdd.com/

21. Wei Q, Keck CM, Müller RH. Oral hesperidin - amorphization and improved dissolution properties by controlled loading onto porous silica. Int J Pharm. 2017;518(1-2):253-63.

22. Silva CC, Miranda CF, Motta MF, Farias JP, Afonso CRM, Ramirez AJ. New insight on the solidification path of an alloy 625 weld overlay. J Mater Res Technol. 2013;2:228-37.

23. Klapper HS, Zadorozne NS, Rebak RB. Localized corrosion characteristics of nickel alloys: a review. Acta Metall Engl Lett. 2017;30:296-305.

24. Mulford SJ, Tromans D. Crevice corrosion of nickel-based alloys in neutral chloride and thiosulfate solutions. Corrosion. 1988;44:891-900.

25. Xie M, Helmink R, Tin S. The influence of Cr on the solidification behavior of polycrystalline γ (Ni)/γ′(Ni3Al)–δ(Ni3Nb) eutectic Ni-Base superalloys. Metall Mater Trans A. 2012;43:1259-67.

26. Sundararaman M, Mukhopadhyay P, Banerjee S. Precipitation of the δ-Ni3Nb phase in two nickel base superalloys. Metall Trans, A, Phys Metall Mater Sci. 1988;19:453-65.

27. Xinxu L, Chonglin J, Yong Z, Shaomin L, Zhouhua J. Segregation and homogenization for a new nickel-based superalloy. Vacuum. 2020;177:109379.

28. Mohrbacher H, Kern A. Nickel alloying in carbon steel: fundamentals and applications. Alloys. 2023;2(1):1-28.